

See discussions, stats, and author profiles for this publication at: <https://www.researchgate.net/publication/221780498>

Sea-ice thickness measurement based on the dispersion of ice swell

Article in *The Journal of the Acoustical Society of America* · January 2012

DOI: 10.1121/1.3662051 · Source: PubMed

CITATIONS

30

READS

131

4 authors:



David Marsan

Université Savoie Mont Blanc

118 PUBLICATIONS 4,250 CITATIONS

[SEE PROFILE](#)



Jerome Weiss

French National Centre for Scientific Research

172 PUBLICATIONS 6,445 CITATIONS

[SEE PROFILE](#)



Eric Larose

French National Centre for Scientific Research-CNRS

176 PUBLICATIONS 5,897 CITATIONS

[SEE PROFILE](#)



J. P. Metaxian

Institute of Research for Development

72 PUBLICATIONS 1,271 CITATIONS

[SEE PROFILE](#)

Some of the authors of this publication are also working on these related projects:



ambient noise [View project](#)



Micro-seismic monitoring of a shear fault within a floating ice plate [View project](#)

Sea-ice thickness measurement based on the dispersion of ice swell

David Marsan^{a)}

ISTerre, CNRS, Université de Savoie, Campus Scientifique, 73376 Le Bourget du Lac Cedex, France

Jérôme Weiss

Laboratoire de Glaciologie et de Géophysique de l'Environnement, CNRS, Université Joseph Fourier, 54 rue Molière, BP 96, 38402 Grenoble Cedex, France

Eric Larose

ISTerre, Université Grenoble 1 CNRS, BP 54, 38402 Grenoble Cedex, France

Jean-Philippe Métaxian

ISTerre, Institut pour la Recherche et le Développement, CNRS, Université de Savoie, Campus Scientifique, 73376 Le Bourget du Lac Cedex, France

(Received 1 July 2011; revised 11 October 2011; accepted 16 October 2011)

The dispersion of flexural waves propagating in the Arctic sea ice cover is exploited in order to locally measure the ice thickness. The observed dispersion, for waves filtered in the 4–20 s period interval, at up to 4 broad-band seismometers deployed in Spring 2007 near the North Pole, is compared to a parameterized model that accounts for a complex wavefield made of a superposition of independent plane waves with different amplitudes and back-azimuth angles. The parameterization, that includes finding the best modeled ice thickness, is performed by using the cross-correlation functions between the seismometers. The ice thickness is estimated to 2.5 ± 0.2 m for the ~ 1 km-large floe the seismic stations were deployed on, which is coherent with other, independent measurements at this site. This study thus demonstrates the feasibility of using broad-band seismometers deployed on the sea-ice in order to passively measure the ice thickness, without requiring active sources nor human intervention. © 2012 Acoustical Society of America. [DOI: 10.1121/1.3662051]

PACS number(s): 43.30.Ma, 43.28.We, 43.40.Dx, 43.50.Rq [RKS]

Pages: 80–91

I. INTRODUCTION

Flexural waves traveling in the sea ice cover are dispersive, the higher the frequency the faster the propagation velocity, at least for periods lower than about 10 s. This dispersion is controlled by the elastic properties of the material, and also by the ice thickness (Ewing *et al.*, 1934; Anderson, 1958). Comparing the observed dispersion of flexural waves with the theoretical dispersion curve could allow the determination of the ice thickness, provided all the elastic constants are known. In seismic studies, the latter can be constrained by estimating the non-dispersive velocities of longitudinal plate (LP) and horizontally polarized shear (SH) waves. Several field experiments have been conducted in the past to exploit these seismic methods (Yang and Giellis, 1994; Stein *et al.*, 1998), see also Anderson (1958) for a review of earlier works. The typical experimental set-up involves the use of active source, e.g., hammer blows or shots; these methods therefore require human assistance and are thus non-autonomous.

For example, Stein *et al.* (1998) used networks of triaxial geophones to invert for ice characteristics, including ice thickness. They generated impulsive signals at a well-defined source location with a sledgehammer, and exploited the travel times of the three phases (P, SH and flexural). The

frequency ranged from 5 to 50 Hz, and the estimates were area-averaged parameters. Performing their inversion on two very different datasets, they obtained good accuracy on the ice thickness for undeformed first-year ice and for more complex, irregular multi-year pack ice, although other characteristics (Young's modulus, shear modulus, and Poisson coefficient) could not be estimated for the latter data.

We here describe how the inversion of ice thickness can be performed without active sources, by exploiting the dispersion of the ice swell. These ubiquitous flexural waves have a narrow spectral content, generally peaking at about 25 to 30 s, and dominate the seismic signal, at least far from the coast. Compared to active sources, the ice swell is a natural, permanent source. The disadvantages in using it are (1) that multiple reflexions and scattering of the ice swell make the wavefield complex to study; (2) that the dominant period is too high to allow for a good resolution of the ice thickness.

To illustrate the second issue, we make use of the phase velocity v_ϕ of flexural waves with angular frequency ω propagating in an ice cover of thickness h lying above an infinitely deep water column, as given by (Stein *et al.*, 1998):

$$\frac{\rho_w}{D} \left(g - \frac{\omega^2}{\sqrt{\frac{\omega^2}{v_\phi^2} - \frac{\omega^2}{v^2}}} \right) = \frac{h\omega^2\rho}{D} - \frac{\omega^4}{v_\phi^4} \quad (1)$$

^{a)}Author to whom correspondence should be addressed. Electronic mail: david.marsan@univ-savoie.fr

where $v = 1440$ m/s is the sound speed in water, $\rho_w = 1000$ kg/m³ is the density of water, $g = 9.81$ m/s² is the acceleration of gravity, ρ is the density of sea ice, and $D = Eh^3/[12(1 - \nu^2)]$ with E Young's modulus and ν the Poisson coefficient of sea ice. For periods much longer than $2\pi\sqrt{h}$, i.e., 6 s to 14 s for a typical ice thickness of 1 to 5 m, the term in brackets in Eq. (1) becomes vanishingly small, and $v_\phi \simeq g/\omega$, the phase velocity of gravity waves, which is independent of the ice thickness. The group velocity v_G is deduced from v_ϕ as

$$v_G = \frac{v_\phi}{1 - \frac{\omega}{v_\phi} \frac{dv_\phi}{d\omega}}. \quad (2)$$

As an example, we show in Fig. 1 the group velocity v_G deduced from v_ϕ for periods ranging between 1 s and 30 s, for various values of the ice thickness. Dependence on the elastic parameters is weak, when probing typical values proposed in the literature for Young's modulus, Poisson coefficient and the density of sea ice. Similarly, the dependence on temperature fluctuations through changes in mechanical properties of the sea ice is even weaker than the effect of changing E from 7.2 to 9.7 GPa as shown in in Fig. 1. For periods greater than about 20 s, hence including most of the energy of the ice swell, the curves collapse onto a single curve $v_G = \frac{g}{4\pi}T$, which is the group velocity of gravity waves. Therefore, the dispersion cannot be used to constrain the ice thickness if we restrict the analysis to the period that are typical of the ice swell: shorter periods must be explored.

In this article, we detail how these two issues can be addressed and check the validity of this method by performing several tests and analyses of field data.

II. DATA

The seismic data analyzed in this work were already described in Marsan *et al.* (2011): a seismic network was deployed in April 2007 as part of the measurement campaign

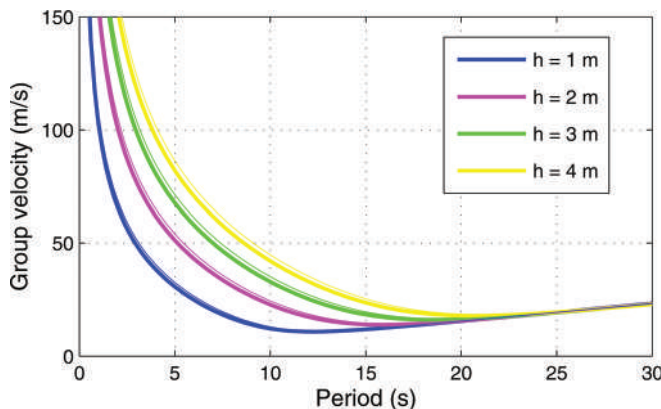


FIG. 1. Group velocity function of period, for flexural waves traveling in an uniform ice plate with varying thickness h as labelled on the graph. Elastic parameters were set to $\rho = 910$ kg m⁻³ (ice density), and $\nu = 0.33$ (Poisson coefficient). Two values of Young's modulus are used: our preferred value of $E = 7.2$ GPa (Stein *et al.*, 1998) as shown in thick lines, and a larger value of $E = 9.7$ GPa, shown in thin line. This value was given by Ponder and Langbein (1964) for low porosity sea ice with less than 10% of brine content.

at the Tara drifting station operating in the framework of the DAMOCLES project (Gascard *et al.*, 2008). From this network made of 16 short-period (1 Hz) vertical seismometers and 5 broad-band Gralp CMG-3ESPC seismometers, we here use data recorded by four of the latter instruments, named thereafter stations 1 to 4. Data from the remaining CMG-3ESPC could not be exploited, as it experienced acquisition problems. Station 4 was located on a different floe from the others. As such, its signal does not correlate as well with the ones recorded by stations 1 to 3. Since the method developed in this work requires a minimum of three stations, we will most of the time discard station 4 from the analysis. We however discuss in Sec. V the effect of adding station 4.

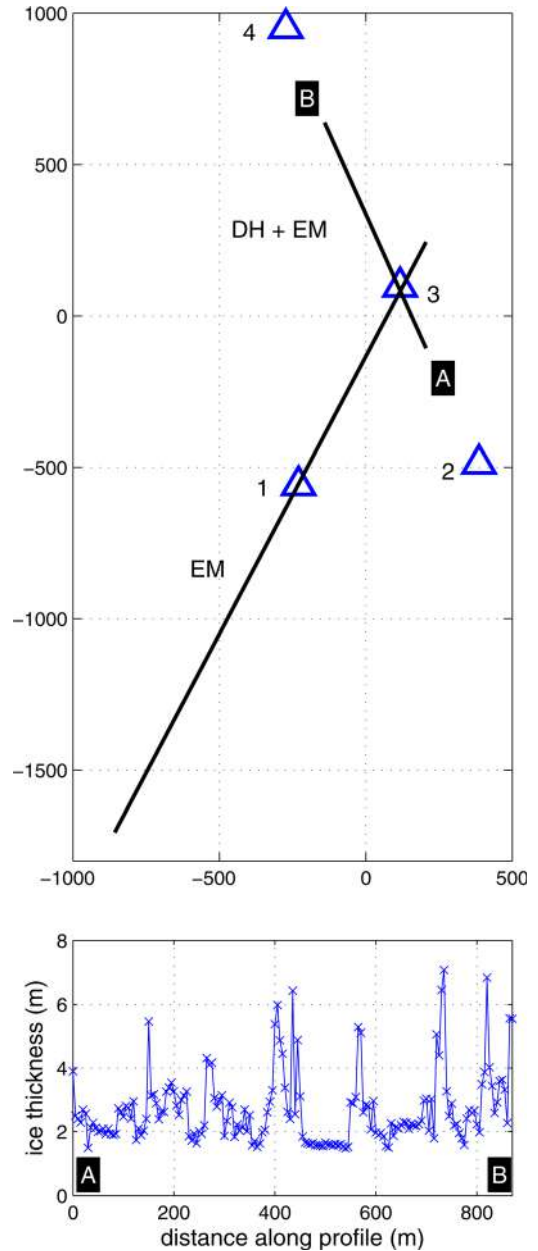


FIG. 2. (Color online) (Top) Relative positions, in meters, of the four seismic stations (labeled 1 to 4), along with approximate positions of the drill-hole (DH) and electromagnetic induction (EM) 800m-long profile, and of the 2160m-long EM profile, see text. The North direction varies with time as the ice floes drift along. (Bottom) Ice thickness from DH measurements along the ~ 800 m-long profile.

The stations were placed at distances of 620 m to 1580 m from each other: denoting by \vec{X}_i the position of station i relative to the center of the array, we have that $\vec{X}_1 = (-229, -558)$, $\vec{X}_2 = (386, -488)$, $\vec{X}_3 = (116, 96)$, and $\vec{X}_4 = (-273, 949)$, all distances being in meters, see Fig. 2.

The broad-band seismometers have a 60 s low frequency cut-off, and their signals were sampled at 100 Hz. We will analyze data acquired between the 27 April and the 25 May 2007, during which stations 1 to 3 operated together (663 hours overall). This duration reduces to 482 h if adding station 4. The network drifted along with the Tara base camp at roughly constant latitude ($88^\circ 14'$ to $88^\circ 32'$) in the Amundsen basin, about 200 km east of the Lomonosov ridge. The water depth is ~ 4000 m there, significantly greater than the maximum wave lengths involved in this study (~ 500 m), justifying the assumption formulated in Sec. I of an infinitely deep water column. No detectable deformation occurred within this network during this time period. We here mostly exploit the vertical displacement rates recorded at these three stations, although results obtained with horizontal displacement rates are discussed in Sec. V.

During this experiment, an independent ice thickness dataset was collected at or close to the location of the array (Haas *et al.*, 2011). On May 8, 2007, drill-hole (DH) measurements were performed every 5 m along a 800 m-long profile, see Fig. 2. An electromagnetic induction (EM) survey was conducted on the same day along the same line, for calibration purposes. Finally, and again at the same date, another EM survey was performed along a close-by 2160-m-long profile. The ice thickness was found to be largely variable along both lines, ranging between about 1.5 m (first-year undeformed ice) to 8 m (pressure ridges), with a mean of 2.70 m (DH) and 2.53 m (EM) for the first profile, and 2.75 m (EM) for the second profile. These mean values are obtained for two lines, and comparison with our estimated area-averaged thickness as detailed in Sec. V should therefore be taken cautiously. They are however likely to be characteristic of the ice floe the three stations 1, 2, and 3 were placed on. Moreover, it should be noted that very little change in ice thickness was observed between May

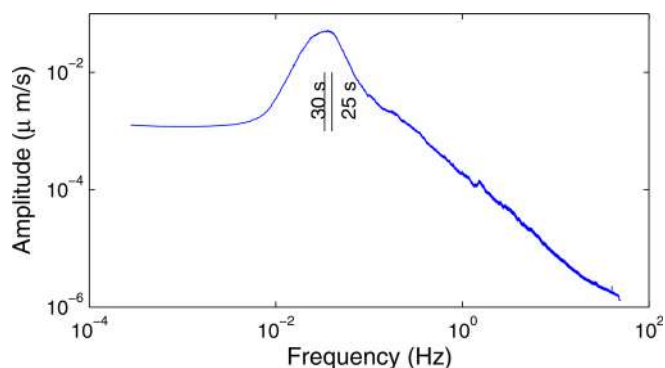


FIG. 3. (Color online) Amplitude spectrum of the vertical displacement rate averaged over the three stations 1–3 and 25 days.

8 and June 26, as shown by a repeat of the survey conducted along the same 2160-m-long line (Haas *et al.*, 2011).

III. ICE SWELL

The broad-band signal is strongly dominated by the ice swell. Computation of the amplitude spectrum gives a peak at periods ranging between 25 and 30 s, see Fig. 3. This spectrum shows some temporal evolution. Indeed, as already pointed out by Wadhams and Doble (2009), distant storms originating in the North Atlantic can generate periods of increased wave amplitude, that then propagate through the ice cover as flexural waves. Given the dispersion of these waves, the arrival time of the high amplitude wavetrains depends on their period.

A spectrogram at long periods, averaged over the three stations 1–3, is shown in Fig. 4. A clear dependence of the arrival time with period is observed at days 141–142 following the increase in significant wave height at latitudes greater than 60° in the North Atlantic Ocean. This dependence can be modeled by assuming a traveling distance of 1400 km in the open ocean and 1600 km through a sea ice cover with 2.7 m of mean ice thickness. A similar, but less remarkable feature is also observed at days 129–130. While an estimate of the ice thickness is feasible on the ground of

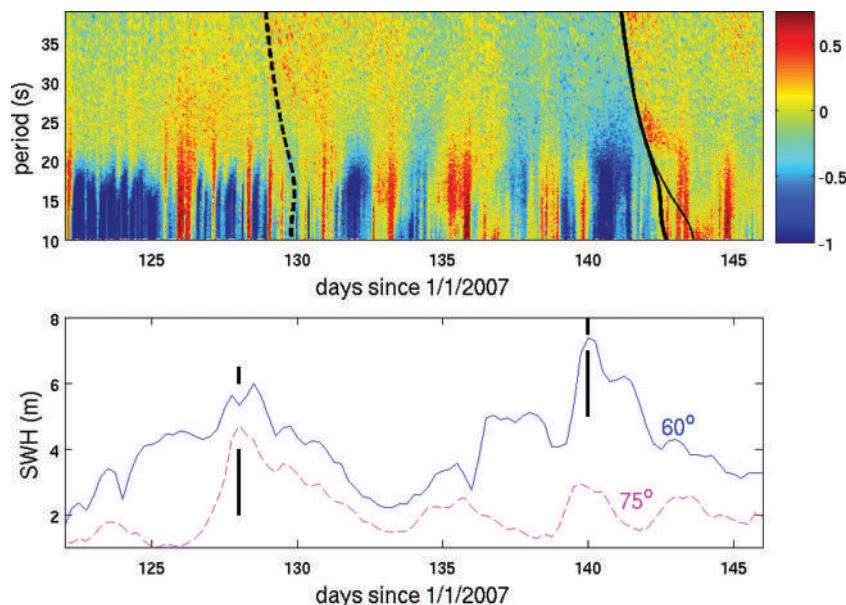


FIG. 4. (Top) Spectrogram for the three stations 1–3. We here show the logarithm (in base 10) of the ratio of the amplitude spectrum computed for 1 h long time windows, over the amplitude spectrum averaged for the 27 days. Thick line: arrival time vs period for waves originating at day 140, 00:00, and propagating over 1400 km in the open ocean and 1600 km through an ice cover with thickness equal to 2.7 m. Thin line: same as thick line, but for an ice thickness of 1 m. Dashed thick line: same as thick line, but for an origin time at day 128, 00:00, and for only 800 km rather than 1400 km of travel in the open ocean, hence for a storm located more to the north. (Bottom) Significant wave height SWH computed using the ERA Interim data of the European Centre for Medium-Range Weather Forecasts, for latitude greater than 60° or 75° , see labels. The origin times of the two storms are shown with vertical lines. Note that the 1st storm occurs more to the north than the second.

these observations, it is however not well constrained: the change in travel time due to ice thickness is most pronounced at periods shorter than about 18 s, for which the signal is too attenuated or scattered to be exploited, see Fig. 4.

IV. METHOD FOR ESTIMATING THE ICE THICKNESS

Here we detail the method developed for estimating the ice thickness from the cross-correlation functions of the vertical signals recorded at the stations. As explained in Sec. IV G, a minimum of 3 stations is required by this method. We therefore describe it for exactly 3 stations; generalization to a larger number of stations is straightforward, and the corresponding results are discussed in Sec. V A.

A. Imaging by correlating seismic noise

Correlating noise between two sensors allows the retrieval of the Green's function that characterizes the propagation of elastic waves, even in the absence of a dominant source, like an earthquake in the case of crustal applications, to illuminate the medium (Weaver and Lobkis, 2001; Lobkis and Weaver, 2001; Campillo and Paul, 2003; Sabra *et al.*, 2005). In the crust, noise with periods in the 10–20 s range has been shown to be primarily caused by ocean swell (Stehly *et al.*, 2006). For Arctic studies, this is clearly the dominant source, as evidenced by the spectral content of the recorded waves, cf. Fig. 3, although the propagation of the swell in a cohesive ice-covered ocean shifts the peak periods to slightly larger values (25 to 30 s, in our case). The feasibility of using noise correlation methods to determine the dispersion of flexural waves, like those associated with the propagation of ice swell, has been evidenced in the case of lab-controlled experiments on plexiglass plates (Larose *et al.*, 2007).

Further complexity arises in our study because of the anisotropy of the sources: the flexural waves come not from one privileged direction, nor from an homogeneous, i.e., isotropic, distribution of sources, but rather from a complex, time-varying distribution, partly controlled by the occurrence of distant storms in the North Atlantic, see Fig. 4. Anisotropic source distributions have been shown to cause asymmetric cross-correlation functions (Larose *et al.*, 2005; Stehly *et al.*, 2006; Froment *et al.*, 2010), so that studying this asymmetry can help estimating the source distribution.

We here develop a method based on a model that reproduces both the temporal and the absolute features of the correlations between stations. It thus allows to invert the anisotropic source distribution, and, more importantly in our application, the flexural dispersion curve, hence the thickness of the ice cover.

B. Cross-correlation functions

We denote by $s_i(t)$ the vertical signal (displacement rate) recorded at station i . The mean Fourier spectrum for the three stations given by $\hat{S}(f) = (|\hat{s}_1(f)| + |\hat{s}_2(f)| + |\hat{s}_3(f)|)/3$, where the symbol $\hat{\cdot}$ denotes the Fourier transform, is shown in Fig. 3.

We first compute the normalized correlation functions $C_{ij}(t)$ between stations i and j with no pre-processing of the

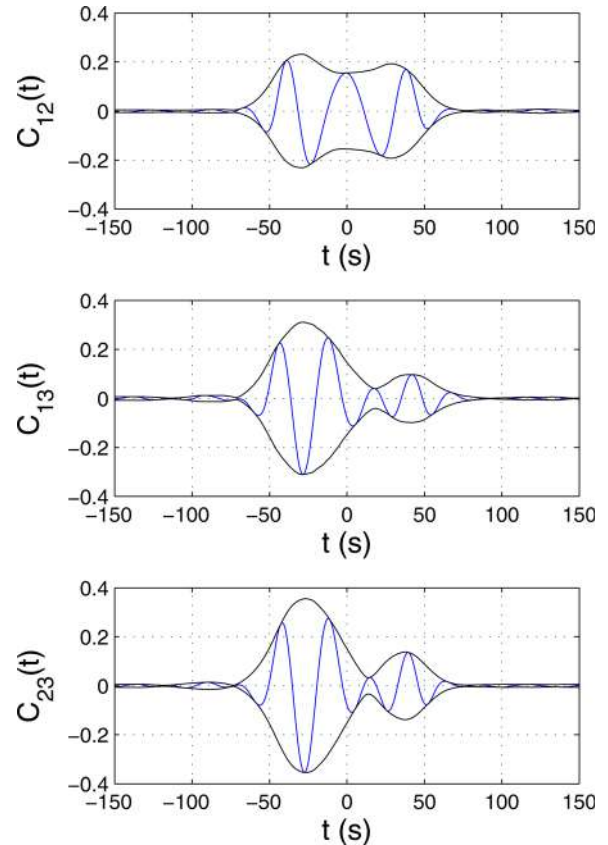


FIG. 5. (Color online) Cross-correlation functions for the three pairs of stations, with no pre-processing. The envelopes are also shown.

waveforms, by inverse Fourier transforming $\hat{C}_{ij}(f) = \frac{1}{N\sigma_i\sigma_j}\hat{s}_i(f)\hat{s}_j^*(f)$, with N the number of samples ($N = 360\,000$ for our 1 h long records sampled at 100 Hz) and σ_i the standard deviation of $s_i(t)$. The normalization by $N\sigma_i\sigma_j$ is done so that $C_{ij}(t)$ is effectively the linear correlation coefficient of s_i and s_j , hence ranging between -1 and $+1$. Compared to previous works on the correlation of seismic noise that do not perform this normalization but instead normalize $C_{ij}(t)$ with $\max_t C_{ij}(t) = 1$, we here exploit the absolute rather than the relative values of $C_{ij}(t)$ as it contains important information that helps constraining the modeling of the complex wavefield.

For each pair (i, j) of stations, we compute $C_{ij}(t)$ on 1 h long records, and average this function over all 663 records. Figure 5 shows the resulting cross-correlations, dominated by a 25 to 30 s period as expected given the Fourier spectrum of Fig. 3. Very similar $C_{ij}(t)$ functions were obtained for one-bit versions of the waveforms (Larose *et al.*, 2004). A clear asymmetry is observed, at least for the 1–3 and 2–3 pairs.

In order to explore frequencies outside the 25–30 s peak, we define band-pass filters $\hat{G}^{(T)}(f) = e^{-(f-1/T)^2/2\Delta f^2}$ centered at frequency $1/T$ and with Δf width. In the following, we will use six such Gaussian filters, with $T = \{4, 5, 7, 9, 12, 20\}$ s center periods, and $\Delta f = \{0.06, 0.05, 0.03, 0.03, 0.01, 0.01\}$ Hz, respectively. Band-pass signals are computed as $\hat{s}_i^{(T)} = \hat{G}^{(T)} \frac{\hat{s}_i}{|\hat{s}_i|}$. These filtered signals preserve the phase of the original signals, and their moduli are equal to $\hat{G}^{(T)}(f)$. This whitening is done to force $s_i^{(T)}$ to have a frequency content effectively centered on T .

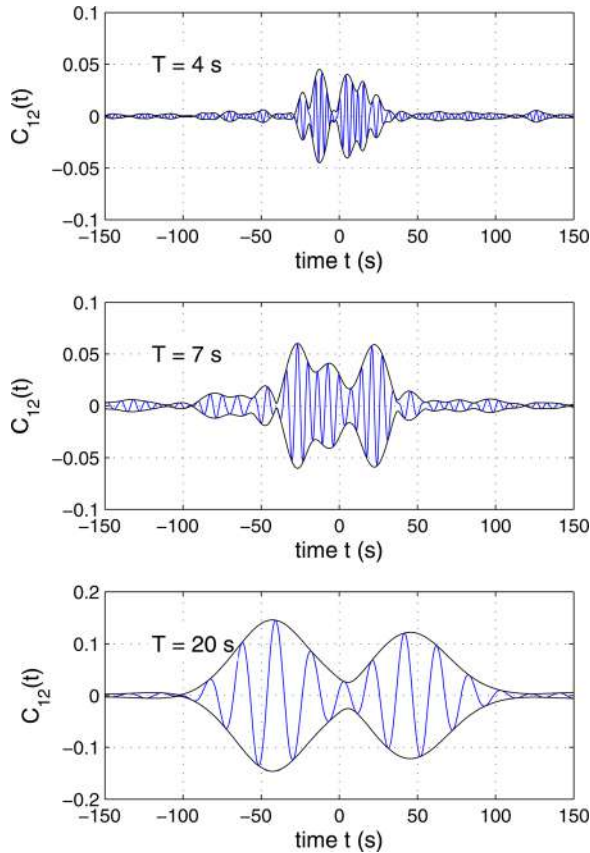


FIG. 6. (Color online) Cross-correlation functions between stations 1 and 2, for three out of the six band-pass filters centered at $T = 4$ s, 7 s and 20 s. The envelopes are also shown.

The cross-correlations $C_{ij}^{(T)}(t)$ between stations i and j for the frequency band centered at $1/T$ are computed from $\hat{C}_{ij}^{(T)}(f) = \frac{1}{N\sigma_i^{(T)}\sigma_j^{(T)}}\hat{s}_i^{(T)}(f)\hat{s}_j^{*(T)}(f)$, where $\sigma_i^{(T)}$ is now the standard deviation of $s_i^{(T)}(t)$. We therefore compute 18 cross-correlation functions (3 pairs of stations, 6 band-pass filters).

We show in Fig. 6 three of the cross-correlation functions between stations 1 and 2, at $T = 4$ s, 7 s and 20 s. We clearly observe that the correlation increases as T increases and becomes closer to the peak period of the ice swell. This implies that, at too low a band-pass filter period T , the correlation becomes too weak, preventing us from using such periods in the estimation of h . Moreover, the maximum of the envelopes is seen to be restricted to short times at low T values, and to spread to longer times at larger T . This is caused by the dispersive nature of the propagation of flexural waves, with propagation velocities decreasing as T increases from 4 s to 7 s and to 20 s.

An estimate of h can be simply determined using the time t_{\max} of this maximum of the envelope, as for example shown in Fig. 6. For the cross-correlation $C_{ij}^{(T)}$, we determine the time $t_{\max,i,j}^{(T)}$ such that

$$\max_t C_{ij}^{(T)}(t) = C_{ij}^{(T)}(t_{\max,i,j}^{(T)}). \quad (3)$$

The group velocity at period T is then estimated as the minimum over the three pairs $\{i,j\}$ of $(|\bar{X}_i - \bar{X}_j|) / (t_{\max,i,j}^{(T)})$. We here keep the minimum, because, for favorable orientations

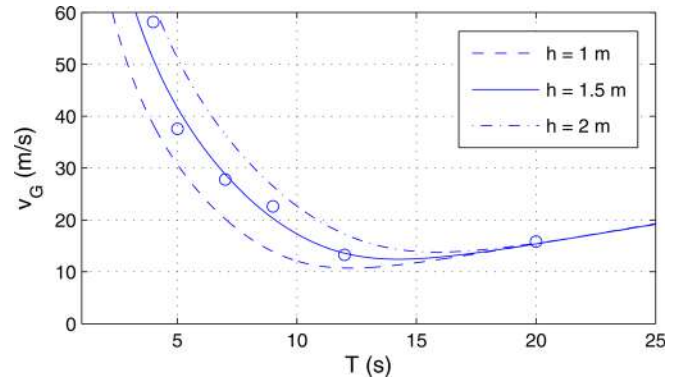


FIG. 7. (Color online) Dispersion curve giving the group velocity v_G in m/s function of the period T in s, as determined using the time t_{\max} of the maxima of the envelopes of $C_{ij}^{(T)}$. The theoretical dispersion curves for $h = 1$, 1.5, and 2 m are shown for comparison.

of the station pair relative to the incoming wavefield, $t_{\max,i,j}$ can be zero, yielding infinite apparent velocities. Figure 7 shows how the estimate of $v_G(T)$ varies with T , and compares this dependence with the theoretical dispersion curve for $h = 1$ m, 1.5 m, and 2 m. A mean thickness of 1.5 m would correctly fit the observations. As we will see in later sections, this estimate is however of poor quality, and does not compare well with the DH and EM measurements. Very similar results are obtained when deconvolving the waveforms from one station by the waveforms recorded at another station, and band-pass filtering the deconvolved signal. This is likely due to the fact that this estimation assumes that the ice swell is a simple plane wave coming from a single direction. This would cause the cross-correlation functions to be strongly asymmetry, with a well-defined maximum close to 1, time-shifted by the time it takes for this wave to propagate from the first to the second station. This model is here clearly not realistic. We therefore drop the assumption that the ice swell is a simple plane wave, and generalize it to the case of a mixture of plane waves with different incoming angles and amplitudes.

C. Model

We now describe how the observed cross-correlation functions $C_{ij}^{(T)}$ can be modeled. Finding the best fit between the observed and modeled functions as a whole, hence considering both the absolute level of correlation and its dependence with time, will allow us in Sec. IV D to estimate the ice thickness h .

Our model considers that the vertical signals at the stations are dominated by the ice swell, which consists in a complex wavefield made of a mixture of independent plane waves with varying incident angle θ relative to our station array. The fact that there is more than just one single incident angle is based on empirical evidence, as in this case the band-pass signals would be shifted in time from one station to the next with a shift depending on the angle between the azimuth of the plane wave and the axis defined by the two stations. The cross-correlation functions would then simply amount to a time-shifted version of $G^{(T)}(t)$, if no significant scattering occurs between the stations. Since this contradicts

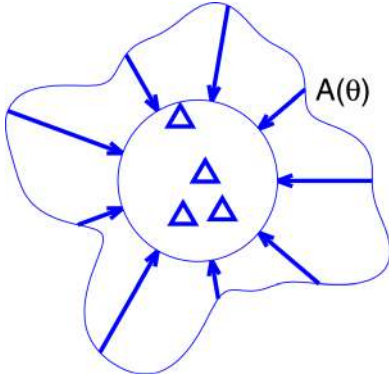


FIG. 8. (Color online) Sketch showing the azimuthal distribution of the incoming wave amplitude $A(\theta)$, relative to the seismic network.

the observations (Fig. 6), we instead assume the ice swell can come from all directions, with an amplitude $A(\theta)$ function of the incident angle, cf. Fig. 8. This mixing of plane waves can be explained by interactions (reflections) of an initial wave with changes in bathymetry or changes in ice thickness and sea-ice concentrations (Squire *et al.*, 2009).

We denote the modeled cross-correlations using the tilde symbol $\tilde{C}_{ij}^{(T)}(t)$. Their Fourier transforms are

$$\hat{C}_{ij}^{(T)}(f) = \frac{|\hat{G}^{(T)}(f)|^2 \mathcal{A}_{ij}^{(T)}(f)}{\int df |\hat{G}^{(T)}(f)|^2 \int d\theta A^2(\theta)} \quad (4)$$

with

$$\mathcal{A}_{ij}^{(T)}(f) = \int d\theta A^2(\theta) e^{i2\pi f \Delta_{ij}^{(T)}(\theta)}. \quad (5)$$

The time delay $\Delta_{ij}^{(T)}(\theta)$ between stations i and j at group velocity $v_G(T)$ for a harmonic plane wave of period T with incident angle θ is simply

$$\Delta_{ij}^{(T)}(\theta) = \frac{(\vec{X}_i - \vec{X}_j) \cdot \vec{u}_\theta}{v_G(T)}, \quad (6)$$

where $\vec{u}(\theta)$ is the unitary vector with incident angle θ .

We emphasize here that direct inspection of the cross-correlation functions, as for example those shown in Fig. 6, is enough to conclude that $A(\theta)$ is neither constant with θ (uniform azimuthal distribution of the incoming ice swell), nor that it is peaked at a given value of θ (one dominant incoming direction). Indeed, for $A(\theta) = A_0 \forall \theta$, hence a uniformly distributed ice swell source, we have $\mathcal{A}_{ij}^{(T)}(f) = 2\pi A_0^2 J_0\left(2\pi f \frac{|\vec{X}_i - \vec{X}_j|}{v_G(T)}\right)$, where J_0 is the Bessel function of the first kind and order 0. Then $\hat{C}_{ij}^{(T)}(f)$ is real, and consequently the cross-correlation function is symmetric in time: $\tilde{C}_{ij}^{(T)}(-t) = \tilde{C}_{ij}^{(T)}(t)$. This symmetry is not observed in Fig. 6, showing that the ice swell azimuthal distribution $A(\theta)$ is non-uniform. As an example, we display in Fig. 9 the cross-correlation $\tilde{C}_{12}^{(T)}(t)$ for $T=20$ s that would be obtained if the distribution $A(\theta)$ were uniform.

Moreover, if $A(\theta) = A_1 \delta(\theta - \theta_1)$, i.e., the ice swell being a simple plane wave coming from direction θ_1 , then

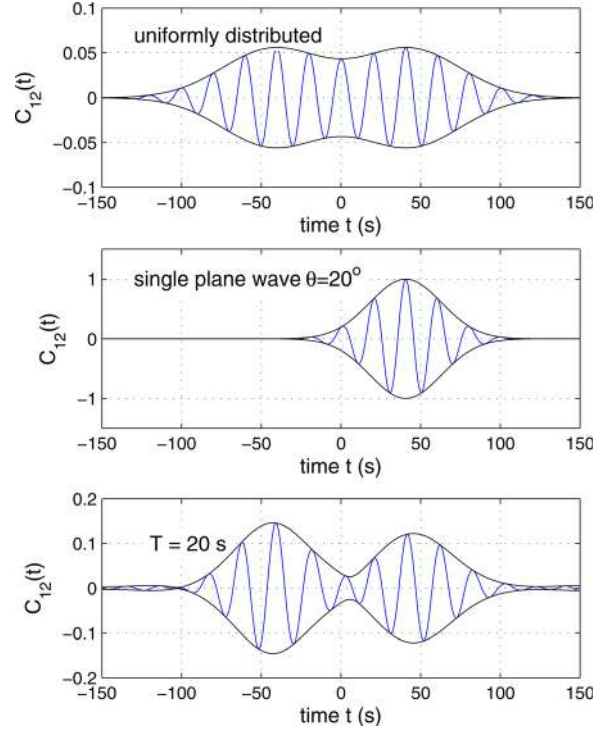


FIG. 9. (Color online) Cross-correlation function $C_{12}^{(T)}(t)$ between stations 1 and 2, for $T=20$ s, along with its envelope, (top) simulated in the case of an ice swell coming from all directions with equal amplitude, (middle) simulated in the case of a single plane wave coming with an angle of 20° relative to the inter-station axis, (bottom) as obtained with the real data—see also Fig. 6. Note that both the absolute value of $C_{12}^{(T)}(t)$ and its dependence on time are affected by changes in the azimuthal distribution $A(\theta)$.

$\tilde{C}_{ij}^{(T)}(t)$ would be the inverse Fourier Transform of $\frac{|\hat{G}^{(T)}(f)|^2}{\int df |\hat{G}^{(T)}(f)|^2}$ shifted by the time it takes for the wave to propagate from station i to station j , hence $\Delta_{ij}^{(T)}(\theta_1)$. In particular, the cross-correlation would then have a peak value equal to 1. This is not observed, cf. Fig. 9 in the case of $\tilde{C}_{12}^{(T)}(t)$ for $T=20$ s obtained with a single plane wave coming with angle $\theta_1 = 20^\circ$, and a 2.5 m thick ice cover.

Finally, we note that the cross-correlation between two stations remains unchanged with varying θ_1 in the case of $A(\theta) = A_1 \delta(\theta - \theta_1)$, as long as $v(T)/\cos \theta_1$ is constant. This trade-off between $v(T)$ and $\cos \theta_1$ thus requires to first determine θ_1 ; as a consequence, the method requires at least 3 stations to correctly estimate both $A(\theta)$ and h .

D. Inversion

The modeled cross-correlation functions are parameterized by the amplitude density $A(\theta)$ and the ice thickness h which controls the group velocity $v_G(T)$. The thickness is the key unknown quantity, and $A(\theta)$ only a by-product of our inversion. The quality of the fit provided by a model $\{A(\theta), h\}$ is measured by a quadratic cost function $J(A, h) = \sum_t \sum_{i,j,T} (\tilde{C}_{ij}^{(T)}(t) - C_{ij}^{(T)}(t))^2$ over the time interval $-150 < t < 150$ s. Note that the cost function is computed using all 18 cross-correlation functions at once.

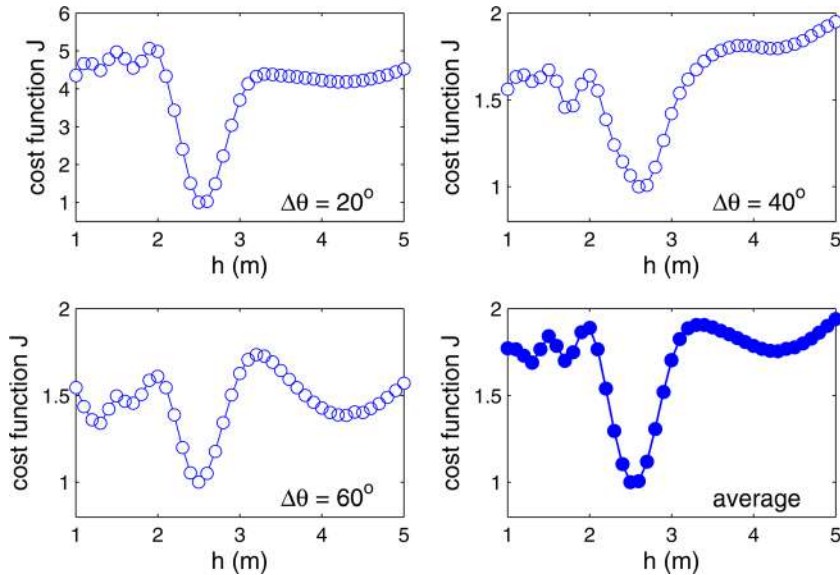


FIG. 10. (Color online) Cost function J vs ice thickness h , for the synthetic test with input $h = 2.5$ m. The angle distribution θ is discretized with $\Delta\theta$ equal to 20° , 40° , or 60° . The cost function obtained by averaging these three cost functions shows a clear minimum at the expected 2.5 m thickness.

We proceed as follows:

- (1) we test regularly spaced values of h , for example $h = 0.1$ m, 0.2 m, ...;
- (2) for each value of h , we invert $A(\theta)$ by minimizing J : $J(h) = \min_A J(A, h)$;
- (3) we search for the minimum of $J(h)$ among all tested values of h .

E. Test for uniform ice thickness

We test the method by inverting synthetic data. We construct the synthetic cross-correlation functions using the same station positions as the actual array, the same band-pass filters as with the real data analysis (see Sec. V for their characteristics), and impose a random azimuthal distribution $A(\theta)$ with the incident angle θ discretized in 9 windows $[0^\circ 40^\circ]$, $[40^\circ 80^\circ]$, etc., hence $\Delta\theta = 40^\circ$. The propagation velocity is computed using an ice thickness $h = 2.5$ m.

It is impossible to *a priori* know from the seismic data how the amplitude distribution $A(\theta)$ should be discretized. The discretization step $\Delta\theta$ must however be specified in our inversion scheme. It seems preferable to have a small $\Delta\theta$, but the smaller this value, the greater the number of amplitude A values to be inverted, and the longer the computation time. Moreover, for any given $\Delta\theta$, spurious local or even global minima can be found, that are however not robust

when changing $\Delta\theta$. We thus adopt the strategy of using several values of $\Delta\theta$; namely, we run 12 independent inversions using different discretizations, and average them all. We use $\Delta\theta = 20^\circ$, 40° , and 60° . For each value of $\Delta\theta$, the “first” window is $[\delta\theta, \delta\theta + \Delta\theta]$ with $\delta\theta/\Delta\theta = 0, \frac{1}{4}, \frac{1}{2}, \text{ or } \frac{3}{4}$.

Figure 10 shows the cost function $J(h)$ for these various discretizations, and for the overall average. The minimum of J is indeed found for $h = 2.5$ m, whatever the discretization step $\Delta\theta$. The inversion is therefore well able to accurately estimate the ice thickness. We reproduce the same test for two other synthetics, after changing the input ice thickness to $h = 1.5$ m and $h = 4$ m. The averaged cost functions shown in Fig. 11 indicate that, in the first case $h = 1.5$ m, an ambiguity exists as two well-marked minima are found (at 1.5 m and 2.2 m), although the latter is only a local minimum. In the second case $h = 4$ m, we find a single minimum, giving an estimate of 3.8 m.

Running 100 simulations with $h = 2.5$ m, and each time inverting for h , gives an estimate $2.5 \leq h \leq 2.8$ m, with a mean of $2.62 \text{ m} \pm 0.09 \text{ m}$. We also tested our hypothesis that $A(\theta)$ is independent of T ; given the limited range of 4–20 s used in this analysis, we do not expect strong changes in the source nor the reflector distributions with varying T . Nevertheless, we ran 100 simulations with $A(\theta)$ randomly drawn separately for all 6 analyzed periods, again with an imposed thickness of 2.5 m. We obtain an estimate of h ranging

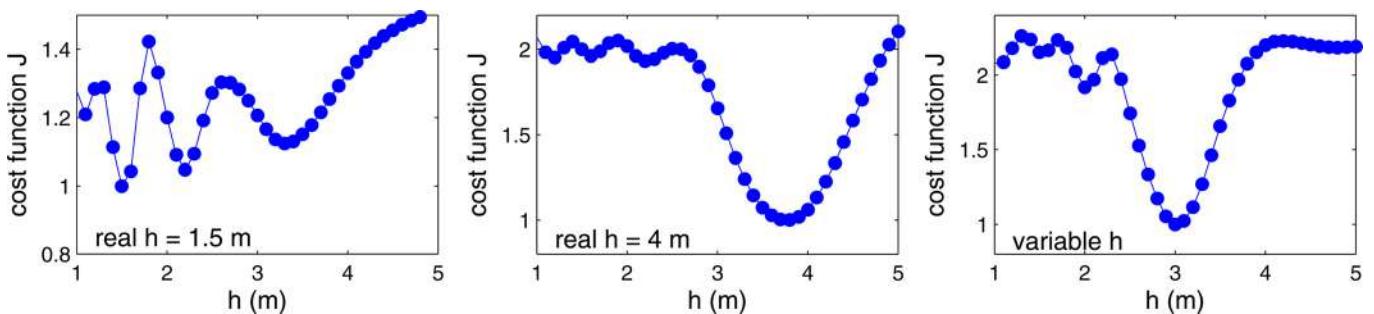


FIG. 11. (Color online) Cost functions obtained by averaging the three cost functions with $\Delta\theta$ equal to 20° , 40° , or 60° , for three synthetic tests constructed with $h = 1.5$ m, $h = 4$ m, and a model with variable ice thickness, see text.

between 2.5 m to 3.1 m, with a mean of 2.81 ± 0.13 m. This unrealistically strong dependence of $A(\theta)$ on T thus causes a slight over-estimation of h .

F. Test for variable ice thickness

The previous test assumed that the ice thickness is uniform, both in the construction of the synthetics and in the inversion itself. This is a strong assumption, as pack ice typically exhibits an heterogeneous distribution, e.g., [Wadhams et al. \(2006\)](#). For the EM and DH profiles conducted close to our seismic stations, the ice thickness has been found by [Haas et al. \(2011\)](#) to vary from 1.5 to 8 m, with a standard deviation of 1.02 m (DH) and 1.11 m (EM, long profile) on May 8, 2007.

We therefore test the inversion, that assumes constant ice thickness, with synthetics constructed with variable ice thickness. We generate the synthetics with a very crude modelling, that consists in using ice thicknesses that are constant for each transect connecting two stations, but variable from one transect to the next. We here take $h = 2.5$ m for the transect between stations 1–2, $h = 4$ m for 1–3, and $h = 3$ m for 2–3.

Figure 11 shows that a global minimum is found at $h = 3.0$ m, instead of local minima at the three values $h = 2.5, 3$, and 4 m. This estimated thickness is not equal to the mean thickness of $\bar{h} = 3.17$ m, although it is not far. Running a series of such tests, by changing the distribution $A(\theta)$, shows that the minimum of $J(h)$ is always within 0.2 m of \bar{h} and is most of the time smaller than it.

These tests therefore indicate that the method is able to give a correct estimate of the mean h , at least with this network geometry, with a typical error not greater than 0.2 m. The quality of the inversion is however likely to depend on the thickness variability: since the inversion assumes uniform thickness, increasing this variability makes the model less adequate to explain the data.

G. Requirements on the network configuration

We investigate how the spacing between the three stations can be optimized in order to provide a good resolution on h . If the stations are too close to one another, then changes in the distribution of $A(\theta)$ will cause very little changes in the cross-correlation functions. To avoid this lack of discrimination, a minimum spacing should therefore be imposed between the stations, that depends on the wavelengths of the ice swell at the peak frequencies of the band-pass filters, ranging from ~ 250 m to ~ 320 m for T between 4 s and 20 s, and $h = 2.5$ m. To find this spacing, we simulate the cross-correlation functions for an equilateral triangle of stations separated by distance ℓ , and check how these functions change when changing the distribution $A(\theta)$. Specifically, we compute the variance of the cross-correlation function at each time sample t in the -150 to 150 s interval, for independent realizations of random $A(\theta)$. The variance averaged over all time samples t defines the sensitivity of the network. Too low a sensitivity means that the same cross-correlation functions are always obtained whatever $A(\theta)$, and therefore that too little information can be extracted from the data to constrain $A(\theta)$, hence also h .

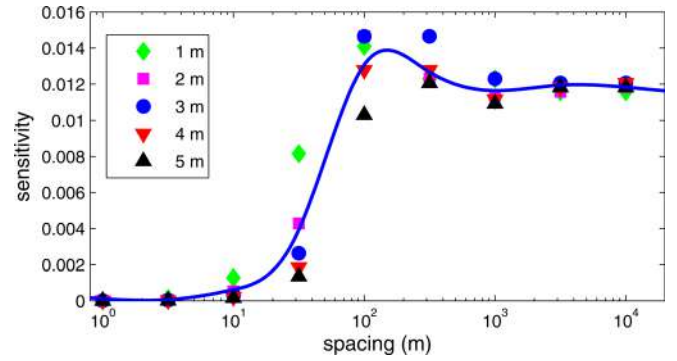


FIG. 12. (Color online) Sensitivity of the cost function on the spacing between the three stations, for different ice thickness ranging from 1 to 5 m (see labels on graph). A spline fit going through the mean sensitivity values is shown.

Figure 12 shows this sensitivity, for ℓ varying between 1 m and 10 km, and for h between 1 and 5 m. We here again use the same band-pass filters as defined above, hence with peak period ranging between 4 and 20 s. The sensitivity is maximum when the spacing is near the minimum wavelength (between ~ 100 m, for $h = 1$ m, to ~ 400 m, for $h = 5$ m) at the tested periods 4–20 s. A spacing of at least 100 m is thus required in order to invert the ice thickness using the ice swell, whatever h . No strong gain in sensitivity is found as ℓ increases past this 100 m value. Note that this analysis does not account for the scattering of the ice swell, that will result in a loss of correlation between stations that are far from one another, so that too large a spacing should be avoided.

V. ANALYSES

A. Ice thickness

We invert the cross-correlation functions as of Fig. 6, that were obtained for the 27 day-long period extending between April 27 and May 25, 2007. As with the test, we use three different angle discretization steps: $\Delta\theta = 20^\circ, 40^\circ$ and 60° , each one with four different initial window (see above). We show in Fig. 13 the three averaged cost functions, and the overall cost function averaged over all 12 distinct angle discretizations. A clear global minimum is found for $h = 2.5$ m, which is coherent with the 2.70 m and 2.53 m mean ice thickness found by the drill-hole and the EM measurements, respectively.

The best fit for the estimated $h = 2.5$ m, and taking $\Delta\theta = 20^\circ$, is shown in Fig. 14 for the 3 (out of 18) cross-correlation functions of Fig. 6. The quality of the fit is very good, especially at long periods T . For this particular discretization of the angles θ , the minimum of J is obtained for $h = 2.6$ m, a value slightly different to the 2.5 m thickness that minimizes the cost function J averaged over all 12 angle discretizations.

The corresponding amplitude distribution $A(\theta)$ is shown in Fig. 15. The distribution is complex, as already suggested by the cross-correlation functions (see Sec. IV B). It is roughly symmetric, with most of the ice swell energy coming from a direction aligned on the Transpolar Drift, hence

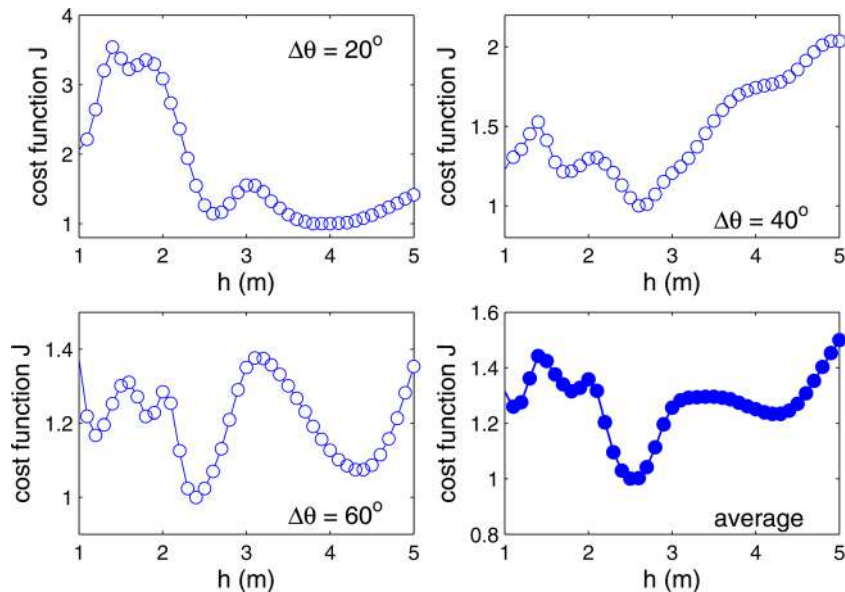


FIG. 13. (Color online) Cost function J vs ice thickness h , for the 27 day-averaged cross-correlations. The angle distribution θ is discretized with $\Delta\theta$ equal to 20° , 40° , or 60° . The cost function obtained by averaging these three cost functions shows a minimum at $h = 2.5$ m.

waves coming from the Siberian Sea and from the North Atlantic Ocean through the Fram Strait.

To test the robustness of the inversion, we use this azimuthal distribution $A(\theta)$ as shown in Fig. 15, and compute the cost function individually for the 3 pairs of stations 1–2, 1–3 and 2–3, with varying ice thickness h . If the inversion is indeed robust, then all 3 pairs should show a clear minimum at the same value of h , proving that this best model is indeed able to explain all cross-correlation functions. Figure 16 shows that the minimum at 2.6 m is effectively robust, with

very little dispersion when considering the 3 pairs of stations individually.

Adding station 4 and reproducing the same analysis, still using $A(\theta)$ of Fig. 15, shows a rather different picture: the minimum of 2.6 m is not robust anymore, as evidenced by the large dispersion in the individual cost function values, see Fig. 16. The distribution $A(\theta)$ and the propagation velocities for $h = 2.6$ m therefore cannot explain all 6 cross-correlations obtained for the 4 stations. This is likely due to a significant change in mean ice thickness for the distinct floe station 4 is located on. We thus conclude that, while adding extra stations could potentially improve the ice thickness estimate, by providing better constraints on the dispersion curve, it can also degrade the quality of the estimate, as is the case here. It is thus important to favor stations located

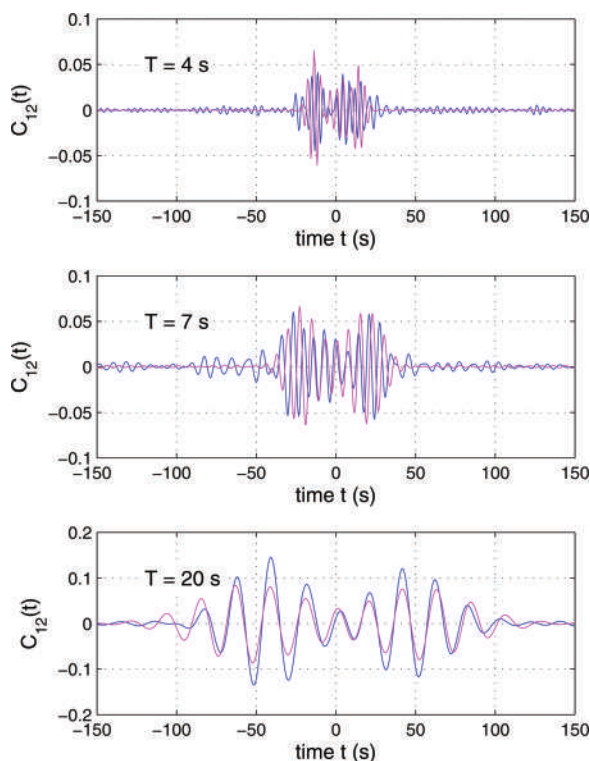


FIG. 14. Simulated cross-correlations for the optimized cost function (in purple) for the three cases shown in Fig. 6 (in blue). We here use an optimal ice thickness of $h = 2.5$ m, and $\Delta\theta = 20^\circ$.

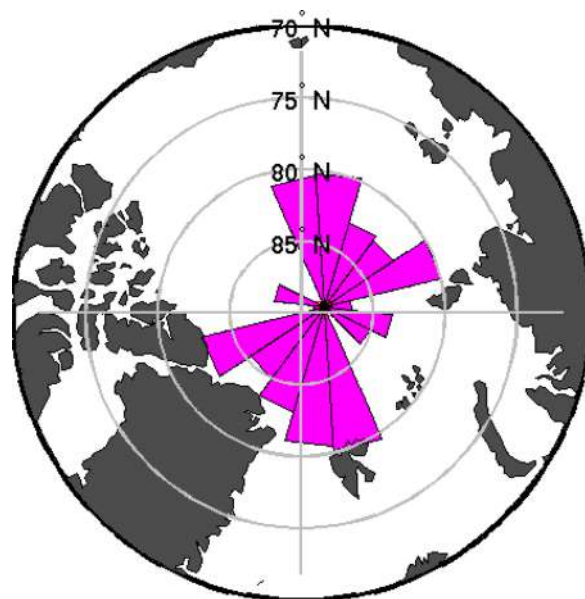


FIG. 15. (Color online) Angular distribution of the ice swell amplitude $A(\theta)$ as given by the best fit of Fig. 14, and an optimized ice thickness $h = 2.5$ m. We here use $\Delta\theta = 20^\circ$.

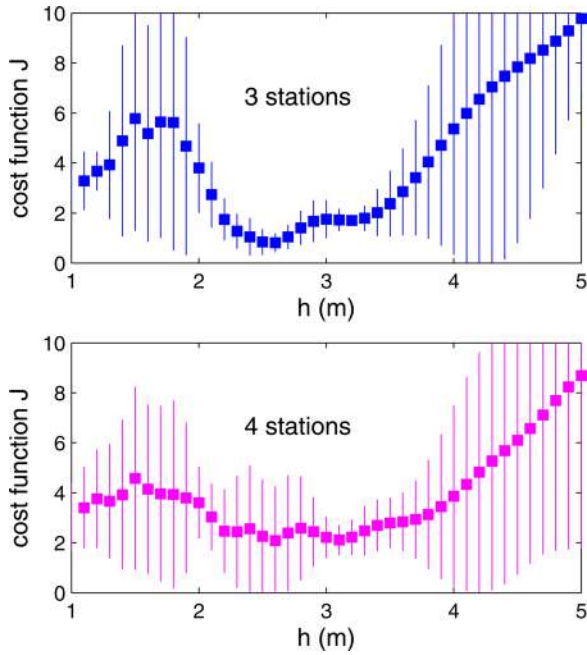


FIG. 16. (Color online) Mean (squares) and standard deviation (error bars) of the individual cost functions for (top) 3 stations and (bottom) 4 stations. The azimuthal distribution $A(\theta)$ is as of Fig. 15.

on a unique floe when using this method. Use of small aperture broad-band arrays deployed on the same floe could help better constraining the azimuthal distribution $A(\theta)$.

Similar analyses on shorter durations, down to only 24 hours, give that $h = 2.5$ m without any resolvable changes (i.e., greater than ± 0.2 m) over the May–June 2007 period. Haas *et al.* (2011) have shown that the ice thickness shrinks by only a few cm over this time period. This change is less than the error of 0.2 m on our estimate, so that it is best to run the analysis on the whole 663 h to maximize the robustness of the estimation.

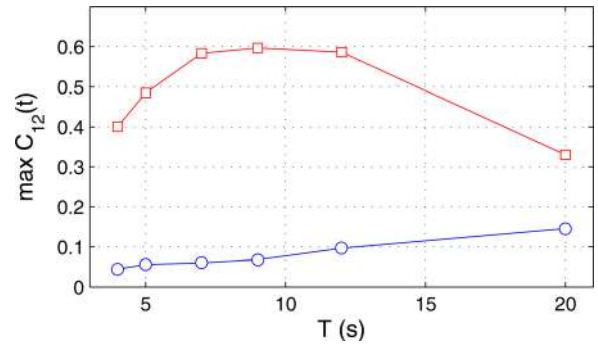


FIG. 17. (Color online) Value of the maximum of the cross-correlation between stations 1 and 2, function of the period of the band-pass filter, for (○) vertical and (□) horizontal displacement rates.

B. Use of horizontal channels

A similar analysis was performed using the horizontal channels of the three stations. Those horizontal channels record horizontal displacement rates in two orthogonal directions. As is detailed in Marsan *et al.* (2011), these recordings show highly coherent episodic low-frequency wavetrains, that were named Low Frequency Bursts (LFB), and which are likely the seismic signature of remote, large-scale shear deformation episodes along major leads. Because of these LFBs, the cross-correlation of horizontal channels is greater than for the vertical displacement rates analyzed so far, see Fig. 17. Moreover, the maximum cross-correlation is obtained for time delays less than 1 s, cf. Fig. 18.

A gain in correlation is potentially interesting, as it gives a better signal to noise ratio, and should therefore reduce the uncertainty in the estimated h . However, LFBs are purely horizontally polarized, and travel at much faster velocity than the ice swell. Although it was not formally proved, several observations suggest that these wavetrains are SH waves, which in the sea-ice cover should propagate non-dispersively at 1600

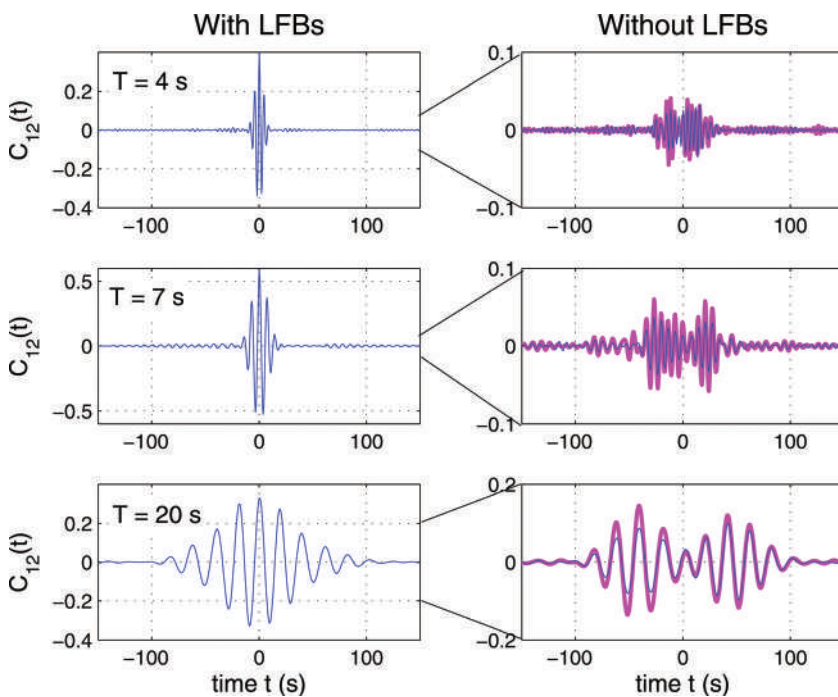


FIG. 18. Cross-correlation functions between stations 1 and 2, using horizontal channels (thin lines) during all 663 h (left graphs) and during the 382 LFB-free hours (right graphs). The cross-correlation obtained with the vertical channel is superimposed on the right-hand graphs (thick lines), and are exactly as those shown in Fig. 6. Note the increase in cross-correlation and the shrinking in the time axis when keeping LFBs.

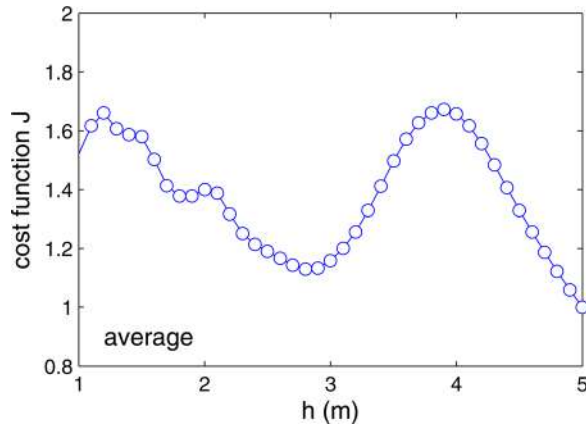


FIG. 19. (Color online) Cost function J vs ice thickness h , for cross-correlation functions obtained with the horizontal channels.

1800 m/s (Marsan *et al.*, 2011). The LFB occurrences being intermittent, the cross-correlations of the horizontal channels average over “quiet” periods, for which the ice swell is dominant, and more energetic periods dominated by LFB occurrences. This mixing of two very different wave phases and propagation velocities explain the general shape of the cost function $J(h)$ for the horizontal channels, see Fig. 19: a local minimum at about 2.8 m, that is possibly a signature of the ice swell dispersion curve, and a global minimum at large $h > 5$ m. For such large thickness, the flexural wave velocities are large (e.g., $v_G = 137$ m/s for $T = 4$ s and $h = 7$ m), and the model is forced to such values in order to explain the apparent very short time delays between the horizontal channels of the three stations.

In order to exploit horizontal channels for measuring the ice thickness, it is therefore necessary to remove the signal due to LFBs. We do this by following the approach described in Marsan *et al.* (2011), that is based on the observation that LFBs typically last several minutes and are clearly seen as anomalously high amplitude wavetrains on the horizontal channels. We thus consider that a 1 h long signal is LFB-free for all three stations if, for the 30 consecutive 2 mn-long windows that can be extracted from this hour, the ratio R of the standard deviation of one horizontal channels with the standard deviation of the vertical channel is never greater than a threshold value R_c . We fix this threshold to $R_c = 3$, cf. Marsan *et al.* (2011). We find that, out of the 633 h used to compute the 6 cross-correlation functions, 281 contain LFBs, and thus 382 are LFB-free. Figure 18 shows that the cross-correlation obtained with horizontal channels during LFB-free periods is very similar to those found with vertical channels during all the 663 h (with and without LFBs), as expected for the flexural mode of propagation of the ice swell. It is therefore easy to remove the influence of the LFBs from the horizontal channels, although there is no particular gain obtained by using these channels, compared to only using vertical channels as we have done so far.

VI. CONCLUSIONS

The feasibility of estimating the area-averaged ice thickness at intermediate scale (100 m to several kms) using seismic instruments with no active sources has been demon-

strated. The ice swell signal is exploited, providing a natural source for analyzing the dispersion of flexural waves with frequency. Compared to active source experiments, this however requires to study a complex wavefield, made of waves coming from different angles rather than from a single source location. This makes for a delicate analysis, and generate uncertainties in the estimated ice thickness. In the case of the Spring 2007 Tara dataset analyzed here, we estimate this uncertainty to be less than 0.2 m, as the minimum of the cost function $J(h)$ shows variations with such an amplitude when exploring the parameter space (azimuthal angle discretization) relevant to this inversion. This uncertainty is also coherent with the typical error found with synthetic tests.

The method requires a minimum of 3 stations, separated by at least 100 m of each other. Too large a spacing can, however, become problematic, as damping and scattering of the wavefield would lead to a lesser correlation between the stations. Moreover, it is necessary to avoid the deployment of stations on distinct floes, as shown by the loss in robustness in the inversion when introducing station 4. This requirement implies that rather compact networks should be favored if using this method. Broad-band seismometers sensing vertical displacements of the ice cover are well designed for this treatment, although horizontal displacements yield similar information if episodic, high amplitude wavetrains (LFBs) related to remote icequakes are removed from the analysis.

ACKNOWLEDGMENTS

We would like to thank Martin Doble, Jari Haapala, Pierre-François Roux, Pierre Rampal, and Guillaume Dumont for discussions, two anonymous reviewers for their constructive comments, and the European Centre for Medium-range Weather Forecasts (ECMWF) for use of the ERA Interim data. This work was supported by the EU FP6 DAMOCLES project.

- Anderson, D. L. (1958). “Preliminary results and review of sea ice elasticity and related studies,” *Trans. Eng. Inst. Canada* **2**, 116–122.
- Campillo, M., and Paul, A. (2003). “Long-range correlations in the diffuse seismic coda,” *Science* **299**, 546–549.
- Ewing, M., Crary, A. P., and Thorne, A. M. (1934). “Propagation of elastic waves in ice,” *Physics* **5**, 165–168.
- Froment, B., Campillo, M., Roux, P., Gouédard, P., Verdel, A., and Weaver, R. L. (2010). “Estimation of the effect of nonisotropically distributed energy on the apparent arrival time in correlations,” *Geophysics* **75**, SA85–SA93.
- Gascard, J.-C., Festy, J., le Goff, H., Weber, M., Bruemmer, B., Offermann, M., Doble, M., Wadhams, P., Forsberg, R., Hanson, S., Skourup, H., Gerland, S., Nicolaus, M., Metaxian, J.-P., Grangeon, J., Haapala, J., Rinne, E., Haas, C., Wegener, A., Heygster, G., Jakobson, E., Palo, T., Wilkinson, J., Kaleschke, L., Claffey, K., Elder, B., and Bottenheim, J. (2008). “Exploring arctic transpolar drift during dramatic sea ice retreat,” *EOS Trans. Am. Geophys. Union* **89**, 21–23.
- Haas, C., Le Goff, H., Audrain, S., Perovich, D., and Haapala, J. (2011). “Comparison of seasonal sea-ice thickness change in the Transpolar Drift observed by local ice-mass balance observations and floe-scale EM surveys,” *Ann. Glac.* **52**, 97–102.
- Larose, E., Derode, A., Campillo, M., and Fink, M. (2004). “Imaging from one-bit correlations of wideband diffuse wave fields,” *J. Appl. Phys.* **95**, 8393–8399.
- Larose, E., Khan, A., Nakamura, Y., and Campillo, M. (2005). “Lunar subsurface investigated from correlation of seismic noise,” *Geophys. Res. Lett.* **32**, L16201.

- Larose, E., Roux, P., and Campillo, M. (2007). "Reconstruction of Rayleigh-Lamb dispersion spectrum based on noise obtained from an air-jet forcing," *J. Acoust. Soc. Am.* **122**, 3437–3444.
- Lobkis, O. I., and Weaver, R. L. (2001). "On the emergence of the Green's function in the correlations of a diffuse field," *J. Acoust. Soc. Am.* **110**, 3011–3017.
- Marsan, D., Weiss, J., Métaixian, J.-P., Grangeon, J., Roux, P.-F., and Haapala, J. (2011). "Low frequency bursts of horizontally-polarized waves in the Arctic sea-ice cover," *J. Glaciol.* **57**, 231–237.
- Pounder, E. R., and Langleben, M. P. (1964). "Arctic sea-ice of various ages II: Elastic properties," *J. Glaciol.* **5**, 99–105.
- Sabra, K. G., Gerstoft, P., Roux, P., Kuperman, W. A., and Fehler, M. C. (2005). "Surface wave tomography from microseisms in southern California," *Geophys. Res. Lett.* **32**, L14311.
- Squire, V. A., Vaughan, G. L., and Bennets, L. G. (2009). "Ocean surface wave evolution in the Arctic Basin," *Geophys. Res. Lett.* **36**, L22502.
- Stehly, L., Campillo, M., and Shapiro, N. M. (2006). "A study of the seismic noise from its long-range correlation properties," *J. Geophys. Res.* **111**, B10306.
- Stein, P. J., Euerle, S. E., and Parinella, J. C. (1998). "Inversion of pack ice elastic wave data to obtain ice physical properties," *J. Geophys. Res.* **103**(C10), 21783–21793.
- Wadhams, P., Wilkinson, J. P., and McPhail, S. D. (2006). "A new view of the underside of Arctic sea ice," *Geophys. Res. Lett.* **33**, L04501.
- Wadhams, P., and Doble, M. J. (2009). "Sea ice thickness measurement using episodic infragravity waves from distant storms," *Cold Reg. Sci. Technol.* **56**, 98–101.
- Weaver, R. L., and Lobkis, O. I. (2001). "Ultrasonics without a source: Thermal fluctuation correlations at MHz frequencies," *Phys. Rev. Lett.* **87**, 134301.
- Yang, T. C., and Giellis, G. R. (1994). "Experimental characterization of elastic waves in a floating ice sheet," *J. Acoust. Soc. Am.* **96**(5), 2993–3009.